Biochimica et Biophysica Acta, 679 (1982) 156–168
Elsevier Biomedical Press

BBA 41002

RADICAL PAIR INTERACTIONS IN SPINACH CHLOROPLASTS

JOHN L. McCRACKEN, HARRY A. FRANK * and KENNETH SAUER

Department of Chemistry and Laboratory of Chemical Biodynamics, University of California, Berkeley, CA 94720 (U.S.A.)

(Received March 4th, 1981)
(Revised manuscript received June 17th, 1981)

Key words: Photosystem I; CIDEP; ESR; Radical pair interaction; Chlorophyll a dimer; Electron acceptor; (Spinach chloroplast)

Time-resolved EPR studies were done on broken spinach chloroplasts under reducing conditions at low temperature (10 K). A dramatic dependence of signal dynamics and lineshape in the *g* 2.00 region on the reduction state of Photosystem I is demonstrated. Computer simulations of the spin-polarized lineshapes obtained in this work suggest that the primary electron acceptor in Photosystem I, a species known as A_1, could be a chlorophyll *a* dimer.

Introduction

Light-induced electron spin polarization is an important consequence of charge separation in the primary photoreactions of photosynthesis. Spin polarization has been studied in a wide variety of green plant [1–4], algal [3–6] and bacterial [7] preparations using EPR techniques at room temperature and at low temperature. All of these studies make use of pulsed-light excitation and fast time-resolved EPR to probe the initial charge-transfer events of the photosynthetic process. The information contained in these measurements is of four types: (a) the structural arrangement of the primary photoreactants with respect to each other and with respect to the membranes in which they reside is reflected in the spectra from flow-oriented [2] or magnetic field-oriented [4] photosynthetic systems; (b) the chemical identities of the donors and acceptors involved in the primary photochemistry of photosynthesis are obtained from the *g* factor and hyperfine coupling constants required to simulate the observed spectral lineshapes [7]; (c) the observed kinetic profiles can be resolved into chemical and spin lattice relaxation dynamics by studying the kinetics of the system as a function of microwave power and temperature [8]; (d) interactions between the photoreactants can be analyzed [9].

We have investigated the low-potential redox dependence of the fast transient EPR signals which are observed in broken chloroplasts and in PS I preparations from spinach. Our choice of sample conditions for this study was based on the current model of the PS I reaction center organization, which may be represented as *P*-700 A_1X Fd_BFd_A [10]. *P*-700 is the primary electron donor. A_1 is thought to be the primary electron acceptor [10]. X is an EPR-characterized species having *g* values of 2.08, 1.88 and 1.78 [11]. Fd_B and Fd_A are iron-sulfur centers which can be reduced chemically by sodium dithionite in the dark [12,13]. X and A_1, which have very low reduction potentials, can be reduced by sodium dithionite plus illumination while freezing to 77 K [14]. Alternative conditions for reducing X and slightly different *g* values for this species have been reported [15–17].

For samples poised in the redox state *P*-700 A_1 X

* Present address: Department of Chemistry, University of Connecticut, Storrs, CT 06268, U.S.A.

Abbreviations: Hepes, *N*-2-hydroxyethylpiperazine-*N'*-2-ethanesulfonic acid; PS, photosystem; Chl, chlorophyll, CIDEP, chemically induced dynamic electron polarization; Fd, ferrodoxin.

0005-2728/82/0000–0000/$02.75

Fd_B^- Fd_A^-, we have essentially duplicated for chloroplasts the results reported by McIntosh et al. [3,4] for algae and subchloroplast particles. However, if the PS I reaction center is poised in the redox state *P*-700 A_1 X^- Fd_B^- Fd_A^- prior to the low-temperature pulsed-light EPR measurement, a substantial change in both dynamics and spectral lineshape of the observed transient species is observed. In our interpretation we attempt to distinguish between two candidates for the primary acceptor A_1, which has been attributed to a Chl *a* monomer [14,18, 19] or dimer [20]. We also raise questions concerning the validity of *g*-value assignments that ignore interactions between the primary photoreactants, and we describe the use of a quantum mechanical model [9] that permits a quantitative analysis of the experimental lineshapes.

Materials and Methods

Time-resolved EPR measurements were made at X-band using a Varian E-109 spectrometer employing 1 MHz magnetic field modulation and equipped with an Air Products Helitran cryostat. The measured response time of the instrument was 2 μs. The Varian TE_{102} cavity (E-231) used in these experiments was fitted with an optical flange made from K-band waveguide to allow 100% transmission of the exciting light. The output of the 1 MHz lock-in amplifier was fed directly into a Nicolet Explorer IIIA Oscilloscope with a Model 204 plug-in. The recorder traces were then transmitted to a NIC-80 minicomputer for signal averaging and analysis.

The light source for these experiments was a Phase-R DL-1400 dye laser operating at 590 nm (Rhodamine 6G in methanol) with a 500 ns pulse width. Typical pulse energies of 100 mJ were utilized, and care was taken to insure that the light was always saturating. The pulse repetition rate was 1 Hz. Temperature measurements were made with a gold/chromel thermocouple.

The possibility of rapid passage distortion of the EPR signals was tested using direct detection of resonance. In these experiments, the magnetic field was not modulated, and the output of the microwave mixer was fed into a wideband amplifier with a bandwidth of 300 Hz–10 MHz and a gain of 30–80 dB. After amplification, the signals were recorded as above. Transient signals which arise from heating of the sample and cavity by the laser flash were eliminated by recording signals on and off resonance and subsequent subtraction after signal averaging. It should be noted that these artifacts arise only accompanying direct detection and are small at the low microwave power levels used in our experiments.

Broken spinach chloroplasts were prepared as described [2] in 0.4 M sucrose, 0.01 M NaCl, 0.05 M Hepes buffer, pH 7.5. After isolation, the chloroplasts were resuspended in 0.2 M glycine buffer, pH 10.1, and treated with 0.2 M EDTA. These resuspensions were then treated in two different ways:

Treatment with dithionite. Chloroplast suspensions were degassed and mixed with sodium dithionite under an N_2 atmosphere so that the concentration of the reducing agent added was 50 mM. Methyl viologen (10 μM) served as a redox mediator.

Treatment with ferricyanide. Chloroplast suspensions were mixed with $K_3Fe(CN)_6$ such that the concentration of the oxidant added was 1 mM.

In some experiments digitonin particles were used instead of broken spinach chloroplasts. These particles were prepared as previously described [22]. In each case, the treated suspensions were combined with an equal volume of ethylene glycol, sealed in EPR tubes, and stored at 77K. Some samples treated with dithionite were poised at a lower redox potential by illumination with a 400 W tungsten lamp during freezing.

Decay constants were obtained from digitized kinetic traces by fitting them with a nonlinear least-squares computer program (ZXSSQ of the IMSL library).

Results

Spinach chloroplasts which were frozen in the dark in the presence of dithionite gave rise to a fast-decaying EPR signal (60 μs at 50 μW microwave power at 10K, see Fig. 1) after a light pulse from a laser. A plot of the amplitude of the EPR transient vs. magnetic field strength is shown in Fig. 2. The spectrum contains both emissive and absorptive components which are observed over a 30 G range near *g* 2.00. This EPR transient is also observed without using field modulation (Fig. 3), and its spectrum exhibits a lineshape that corresponds to the first derivative seen using field modulation (Fig. 2).

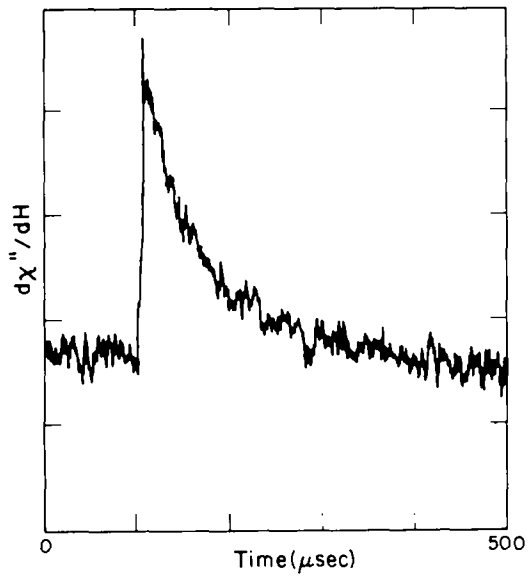

Fig. 1. EPR transient signal from broken spinach chloroplasts suspended under N_2 gas in 0.2 M glycine buffer, pH 10.1, treated with 50 mM sodium dithionite, 10 μM methyl viologen, and ethylene glycol before freezing in the dark. The spectrometer settings were: microwave power, 50 μW; temperature, 10 K; field modulation frequency, 1 MHz; modulation amplitude, 4G; field position, g 2.005. This trace is the average of 400 events.

Because there is qualitative agreement between the lineshapes in Figs. 2 and 3, we conclude that rapid passage effects owing to field modulation detection

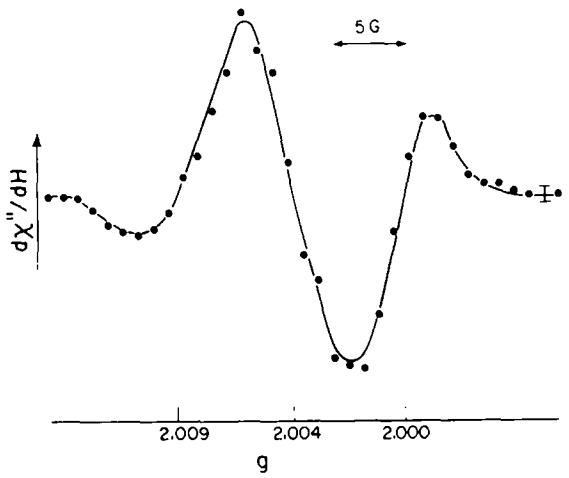

Fig. 2. A plot of transient signal amplitude versus magnetic field strength for broken spinach chloroplasts prepared as in Fig. 1. The conditions for the measurement were identical to those given in Fig. 1 (sweep time 500 μs).

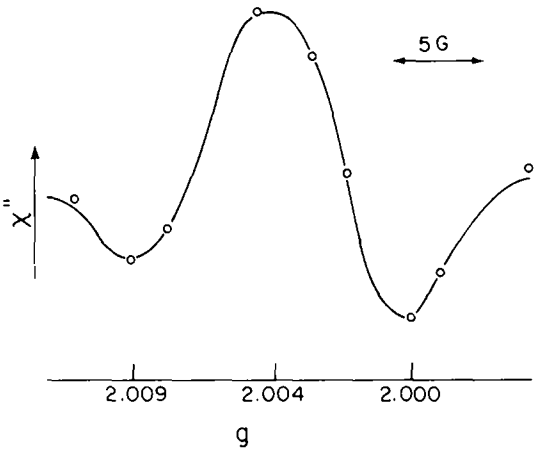

Fig. 3. A plot of transient signal amplitude vs. magnetic field strength for broken spinach chloroplasts prepared as in Fig. 1. The conditions for the measurement were: microwave power, 50 μW; temperature, 10 K, and direct detection of the EPR transient was utilized. 400 events were averaged at each field position (sweep time 500 μs).

of the transient amplitudes are small. Furthermore, these rapid transient signals do not decay directly to zero. When examined at longer (millisecond) times after the laser pulse, the signals cross the baseline and decay to a low level only after approx. 1 ms

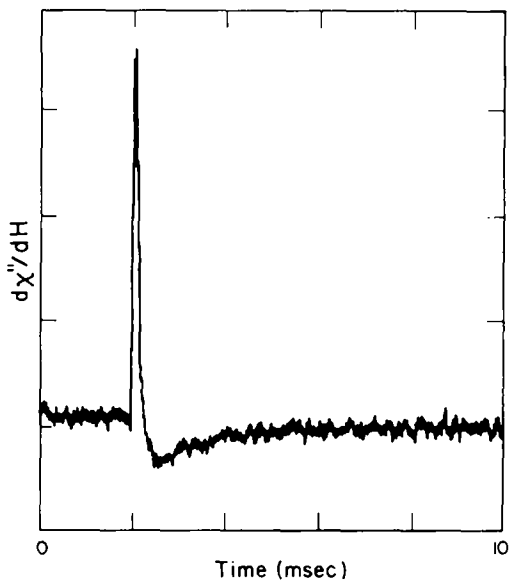

Fig. 4. EPR transient signal identical to that of Fig. 1 except that the sweep time of the transient recorder has been lengthened to 10 ms.

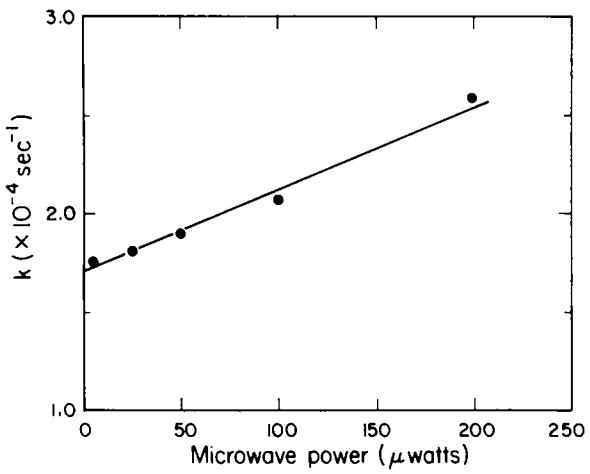

Fig. 5. Plot of the decay constant vs. microwave power for the rapid transient signal displayed in Fig. 1. These data were obtained using field modulation. The decay constants were obtained by fitting the digitized data to a single exponential using a nonlinear least-squares computer program (sweep time 500 μs).

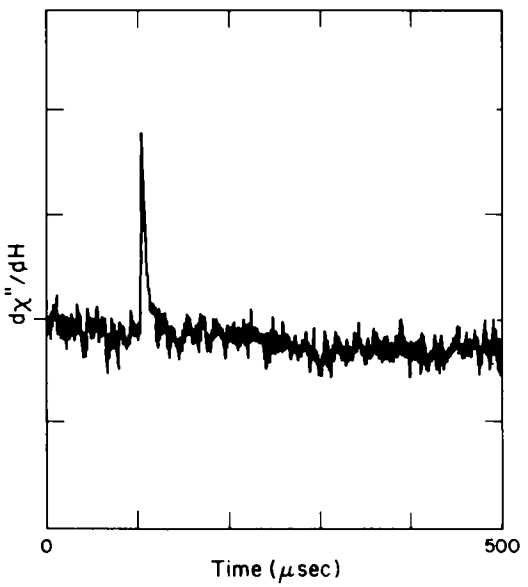

Fig. 6. EPR transient signal from broken spinach chloroplasts suspended under N_2 gas in 0.2 M glycine buffer, pH 10.1, treated with 50 mM sodium dithionite, 10 μM methyl viologen and ethylene glycol. The sample was then frozen during illumination with a 400 W tungsten lamp. The spectrometer settings for this measurement were: microwave power, 50 μW; temperature, 10 K; field modulation frequency, 1 MHz; field modulation amplitude, 4 G; field position, g 2.004. This trace was the average of 400 events.

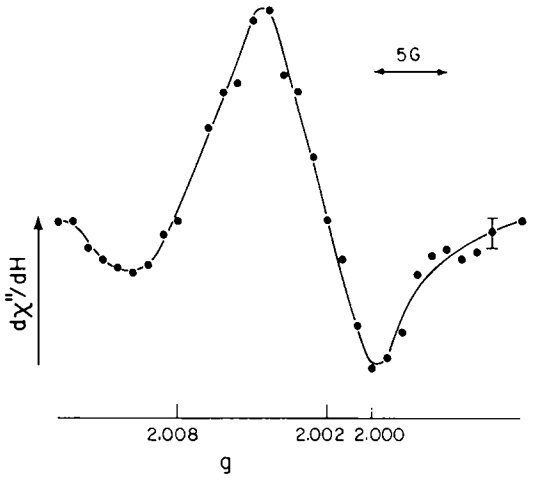

Fig. 7. A plot of transient signal amplitude vs. magnetic field strength for broken spinach chloroplasts prepared as in Fig. 6. The spectrometer settings were identical to those of Fig. 6 (sweep time 500 μs).

(Fig. 4). Both of these kinetic components show a dependence on microwave power and temperature. A plot of the dynamics of the faster component vs. microwave power is given in Fig. 5.

Chloroplasts or digitonin-treated PS I particles prepared in the state P-700 A_1 X^- Fd_B^- Fd_A^- by freezing under illumination in the presence of dithionite gave rise to a much faster decaying transient (6 μs at 50 μW microwave power at 10 K; Fig. 6) after a light pulse from a laser. The relaxation time

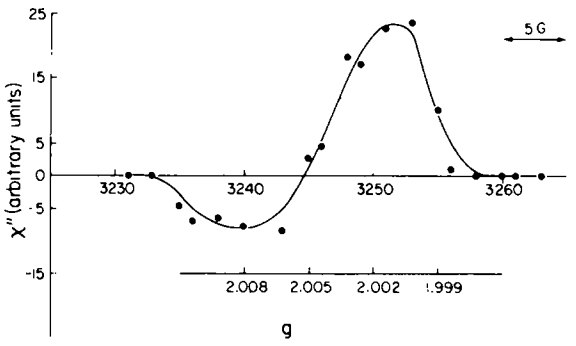

Fig. 8. A plot of transient signal amplitude vs. magnetic field strength for broken spinach chloroplasts prepared as in Fig. 6. The spectrometer settings were: microwave power, 50 μM; temperature, 10 K; direct detection; and gain, 80 dB. The kinetic traces from which the points were obtained were the average of 400 events.

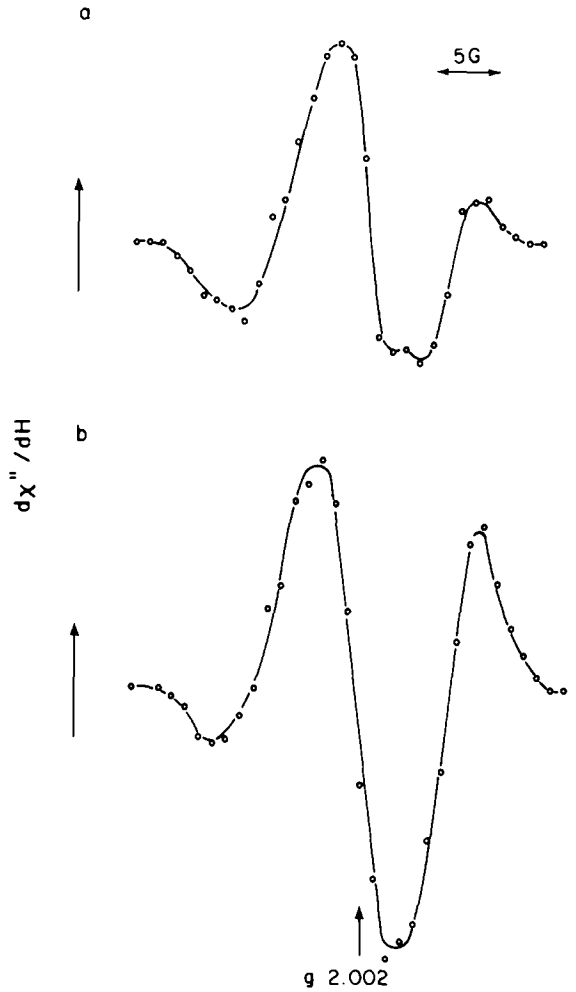

Fig. 9. Plots of EPR transient amplitude vs. magnetic field strength for magnetically aligned, broken spinach chloroplasts. Samples were prepared under N_2 gas in 0.2 M glycine buffer, pH 10.1, treated with 50 mM sodium dithionite, 10 μM methyl viologen and mixed with an equal volume of ethylene glycol before freezing in the dark in a 10 kG alignment field. The spectrometer settings were: microwave power, 50 μM; temperature = 10 K; field modulation frequency, 1 MHz; modulation amplitude, 4 G. Each point represents the average of 400 events. In a the sample was placed in the spectrometer so that the Zeeman field was parallel to the alignment field, and in b the alignment and Zeeman fields are perpendicular.

of this transient signal decreases to 2 μs (our instrumental time resolution limit) as the microwave power is raised to 100 μW. A plot of the amplitude of the transient signal (observed using field modulation) vs. magnetic field strength (Fig. 7) reveals a mixed emissive and absorptive pattern which is significantly different from the spectrum shown in Fig. 2. The transient EPR spectrum of chloroplasts prepared in this condition was also observed using direct detection (Fig. 8). However, no longer-lived (millisecond) component is observed at longer sweep times in these samples.

An orientation effect of the transient spectra was observed on magnetically aligned chloroplasts (alignment field strength 10 kG), but only for those prepared in the redox state, *P*-700 A_1 X Fd_B^- Fd_A^- (Fig. 9). Transient EPR signals identical to those shown in Figs. 1 and 6 were observed in PS I-enriched preparations. No transient EPR signals were observed in the *g* 2.00 region of spinach chloroplasts which had been treated with $K_3Fe(CN)_6$, thereby oxidizing *P*-700 to *P*-700$^+$.

Discussion

The observation of polarized EPR signals arising from PS I of spinach chloroplasts at room temperature has been reported [1,2]. Those results were quantitatively explained by Friesner et al. [9], who developed calculations on a system of membrane-bound radicals based on the radical pair theory of CIDEP developed by Adrian [21]. In this section a brief review of the radical pair mechanism and its adaption to photosynthetic systems will be given. We will then utilize the results to obtain computer simulations of the data presented above.

The spin Hamiltonian for a weakly coupled radical pair created by an electron transfer from a donor molecule (D) to an acceptor (A) can be written as:

$$\mathcal{H}_{RP} = \beta \boldsymbol{H}_0 \cdot [\boldsymbol{g}_D \cdot \boldsymbol{S}_D + \boldsymbol{g}_A \cdot \boldsymbol{S}_A] - J(2\boldsymbol{S}_D \cdot \boldsymbol{S}_A + \tfrac{1}{2}) + \sum_i A_i^{(D)} \boldsymbol{I}_i^{(D)} \cdot \boldsymbol{S}_D + \sum_j A_j^{(A)} \boldsymbol{I}_j^{(A)} \cdot \boldsymbol{S}_A \qquad (1)$$

where β is the Bohr magneton, $\boldsymbol{H}_0$ the applied magnetic fied vector $\boldsymbol{g}_D$ and $\boldsymbol{g}_A$ the *g* tensors for the donor and acceptor species, $\boldsymbol{S}_D$ and $\boldsymbol{S}_A$ the spin operators for the donor and acceptor, respectively, *J* the magnitude of the isotropic exchange interaction between the two radicals and the last two terms represent the isotropic hyperfine interaction for each radical. The eigenstates of this Hamiltonian have been determined by Friesner et al. [9] assuming that *g*-value

anisotropy is small and that the spin states are quantized in the direction of the effective field

$$h' = H_0 (g_A + g_D) \tag{2}$$

Their results, which are analogous to those of Adrian [21], are:

$$\phi_1 = [(\omega + J)/2\omega]^{1/2}|S\rangle + [(\omega - J)/2\omega]^{1/2}|T_0\rangle \; ; E_1 = \omega$$

$$\phi_2 = [(\omega - J)/2\omega]^{1/2}|S\rangle - [(\omega + J)/2\omega]^{1/2}|T_0\rangle \; ; E_2 = -\omega$$

$$\phi_3 = |T_{+1}\rangle \; ; E_3 = \tfrac{1}{2}\beta H_0 \cdot (g_D + g_A) \cdot \hat{z} + \tfrac{1}{2}\left(\sum_i A_i^{(D)} m_{iz}^{(D)} + \sum_j A_j^{(A)} m_{jz}^{(A)}\right) - J$$

$$\phi_4 = |T_{-1}\rangle \; ; E_4 = -E_3 - 2J \tag{3}$$

where $|S\rangle$, $|T_{+1}\rangle$, $|T_0\rangle$, $|T_{-1}\rangle$ are the singlet-triplet spin functions, and $\omega = [H_{AD}^2 + J^2]^{1/2}$. H_{AD} is the off-diagonal matrix element between the $|S\rangle$ and $|T_0\rangle$ states and is given by

$$H_{AD} = \langle S|\mathcal{H}_{RP}|T_0\rangle = \tfrac{1}{2}\beta H_0 \cdot (g_D - g_A) \cdot \hat{z} + \tfrac{1}{2}\left(\sum_i A_i^{(D)} m_{iz}^{(D)} - \sum_j A_j^{(A)} m_{jz}^{(A)}\right) \tag{4}$$

$\hat{z}$ in the above equations is a unit vector in the direction of the effective field and $m_{iz}^{(n)}$ is the z component of the nuclear spin of the i^{th} nucleus on molecule n. One should also note that the neglect of S-$T_{\pm 1}$ mixing in Eqn. 3 has been shown to be reasonable in this system [9].

The polarization, ρ, on either radical can be obtained by determining the time evolution of the radical pair wave function and computing the expectation value of the spin angular momentum quantized in the direction of the effective field. Thus, the polarization on the donor radical would be given by:

$$\rho_{D^+}(t) = 2\langle\psi(t)|S_z^{(D)}|\psi(t)\rangle \tag{5}$$

Our choice of experimental conditions for this study requires the use of both one- and two-site models for development of spin polarization in membrane-bound systems proposed by Friesner et al. [9]. For experiments where X is reduced, only the initial electron-transfer reaction can occur; the resulting spin polarization arises from spin-spin interactions between P-700$^+$ and A_1^-. This situation is described by the so-called one-site model. For the case where X is not reduced prior to flashing, charge transfer occurs from P-700 to A_1, to form the P-700$^+A_1^-$; radical pair, and then from A_1^- to X, to form the P-700$^+$ X$^-$ radical pair. Previous work [2,9] has shown that X is close enough to P-700 for a small spin-spin interaction to exist for the P-700$^+$ X$^-$ radical pair. In this case, spin polarization on P-700$^+$ develops from interactions with both A_1^- and X$^-$. Here, a two-site model for the development of spin polarization is required.

One-site model

As stated above, the one-site model is applicable when spin polarization develops on a radical due to spin-spin interactions with a single second radical. This model is applicable to the experimental case where X is reduced prior to flash stimulation. To compute the polarization, ρ, one first determines $|\psi(0)\rangle$, the radical pair wave function upon creation of the pair by charge separation, and then uses the time-dependent Schrödinger equation to obtain $|\psi(t)\rangle$. Once $|\psi(t)\rangle$ is obtained, $\rho(t)$, the polarization for a time interval t during which J is constant can be computed using Eqn. 5.

It is well established that the radical pair in these systems is created in a singlet state [22]. Therefore, $|\psi(0)\rangle = |S\rangle$ and it follows that:

$$|\psi(t)\rangle = [(\omega + J)/2\omega]^{1/2} e^{-\omega t/\hbar}|\phi_1\rangle + [(\omega - J)/2\omega]^{1/2} e^{i\omega t/\hbar}|\phi_2\rangle \tag{6}$$

Using this result in Eqn. 5 yields:

$$\rho_{D^+}(t) = (2H_{AD}J/\omega^2)\sin^2\omega t \tag{7}$$

for the polarization on the donor species. As noted by Friesner, et al. [9], this expression is significant in photosynthetic systems because the lifetime of the radical pair can be quite long, especially in cases where charge transfer is blocked by poising the reaction center at low oxidation-reduction potentials. In systems of diffusing radicals the lifetime of the radical pair is a few picoseconds, and this term is neglible [21].

The probability that the radical pair $P\text{-}700^+A_1^-$ will exist for time t is given by $(dt/\tau_1)e^{-t/\tau_1}$ where τ_1 characterizes the lifetime of the radical pair. Multiplying this probability by Eqn. 7 and integrating over time yields the time-averaged polarization for the one-site model:

$$\rho_{D^+}(\tau_1) = 4H_1J_1\omega_1{}^2/(1+4\omega_1{}^2\tau_1{}^2) \tag{8}$$

where H_1 is the off-diagonal element H_{AD} for the radical pair $P700^+A_1^-$, J_1 the value of the exchange integral for this pair and $\omega_1 = (H_1{}^2 + J_1{}^2)^{1/2}$.

Application of the one-site model

Illumination while freezing the chloroplasts in the presence of sodium dithionite not only reduces X to X^- but also is reported to reduce A_1 to A_1^- [18]. However, because of the low potential of the A_1/A_1^- couple and because we observe a transient EPR signal following a pulse of light in PS I-enriched preparations, it appears that A_1 is not fully reduced under our conditions. We conclude that the spectrum shown in Fig. 7 arises from either a convolution of polarized $P\text{-}700^+$ and A_1^- signals or that the observed spectrum is representative of polarized $P\text{-}700^+$ alone. The second hypothesis assumes that the polarized spectrum of A_1^- is broadened by spin-spin interactions with X^- and is therefore unobservable in this case. There is precedence for this idea in bacterial photosynthesis where polarized g 2.00 signals are unobservable until the Fe is removed from the reaction center [7].

We will first examine the case where the polarized spectrum of Fig. 7 is assumed to be due to $P\text{-}700^+$ alone. As stated above, no detectable orientation dependence in magnetically aligned chloroplasts was observed for broken chloroplasts in this redox state. This indicates that contributions from anisotropic g tensors or other anisotropic interactions are negligible. The absence of anisotropic species at this stage in PS I electron transport is consistent with the idea that A_1 is a chlorophyll species.

The experimental EPR intensity of $P\text{-}700^+$ as a function of magnetic field strength, H, is given by:

$$I_{P\text{-}700^+}(H) = \sum_i -(\bar{\rho}_i)\, e^{(H-H_i^0)^2/\delta^2} \tag{9}$$

(all hyperfine states of $P\text{-}700^+$)

where H_i^0 is the center field position of hyperfine line i and δ the intrinsic width of each hyperfine line. $\bar{\rho}_i$ is the time-averaged polarization of hyperfine line i and is obtained from Eqn. 8. One should note that $\bar{\rho}_i$ is a function of hyperfine states on both $P\text{-}700^+$ and A_1^- because H_1, the off-diagonal element H_{AD} for this radical pair, is given by:

$$H_1^{ij} = \tfrac{1}{2}(g_{P\text{-}700^+} - g_{A_1^-})\,\beta H_0 + \tfrac{1}{2}(A_j^{(P\text{-}700^+)}\, m_{jz} - A_j^{(A_1^-)}\, m_{jz}) \tag{10}$$

Therefore, for the purpose of calculation, Eqn. 8 can be rewritten as:

$$\bar{\rho}_i(\tau_1) = \sum_j 4H_1^{ij}J_1\tau_1^2/(1+4(\omega_1^{ij})^2\,\tau_1^2) \tag{11}$$

(all hyperfine states of A_1^-)

where $\omega_1^{ij} = ((H_1{}^{ij})^2 + J_1{}^2)^{1/2}$. Another point is that for $\bar{\rho}_i > 0$, hyperfine line i will be found in emission, since ρ is defined as the population difference between state α and state β. This is the reason for the minus sign in Eqn. 9.

To test the hypothesis that A_1 is a Chl *a* dimer or monomer, computer simulations of the possible polarized $P\text{-}700^+$ spectra were done using the above analysis. Two sets of simulations were done. In the first set the radical pair consisted of a Chl *a* dimer cation and a Chl *a* dimer anion, while in the second set of simulations the radical pair consisted of a Chl *a* dimer cation and a Chl *a* monomer anion. The g values and hyperfine coupling constants for $P\text{-}700^+$ and A_1^-; in our simulations were taken from the literature [23,24]. The best simulations for each set (A_1 = Chl *a* dimer anion, A_1 = Chl *a* monomer anion) are shown in Fig. 10. The criteria for choosing good fits to the data are the splittings between the peaks and their relative amplitudes. We found that these features could be nicely predicted by both the dimer anion and monomer anion models. In the case where A_1^- is taken to be a Chl *a* dimer anion, a small g value difference ($\Delta g = g_1 - g_2 = -0.0005$) was required to obtain the proper asymmetry in the polarized $P\text{-}700^+$ spectrum. The asymmetry in this case is also moderately affected by J, and a J value of 1.5 G gave the best fit for g_{A_1} 2.0031. For the case where A_1^- is taken to be a Chl *a* monomer anion, we found a more

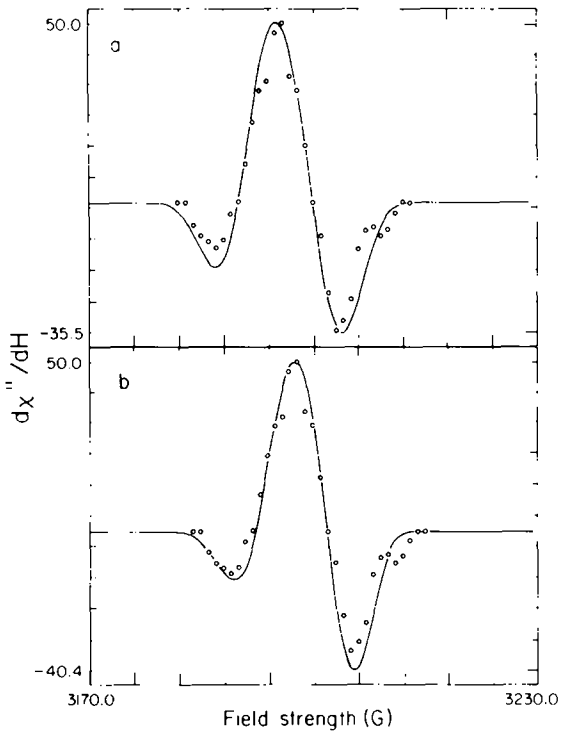

Fig. 10. A comparison of calculated and experimental EPR spectra for the data of Fig. 7. The calculated lineshape represents polarization developed on P-700$^+$ via a 'one-site' interaction with (a) Chl a monomer anion species and (b) Chl a dimer anion species. For both simulations the g value of P-700$^+$ was taken to be 2.0026; the hyperfine coupling constants for P-700$^+$ were 2.10 G (four protons) and 1.3 G (six protons); and the radical pair lifetime, τ_1, was set at 10 μs. For curve a the g value of the Chl a monomer was 2.0035, the hyperfine coupling constants considered were 4.9 G (three protons) and 1.70 G (three protons) and J_1 = 2.00 G. For curve b the g value of the Chl a dimer anion counter-radical was 2.0031, the hyperfine coupling constants utilized were 2.45 G (six protons) and 0.85 G (six protons) and J_1 = 1.50 G. For curve a, the experimental points were shifted downfield 2 G to correlate with the predicted lineshape.

negative Δg of -0.0009 was required to obtain the correct asymmetry. In the monomer case, J also affects the asymmetry but to a much lesser degree than for the dimer model. A J value of 2.0 G gave the best results in this instance. In both sets of simulations, τ_1, the radical pair lifetime, was set at 10 μs, the approximate decay time of the EPR transient for this sample condition. As one might expect, τ_1 was found to have a negligible effect on the relative peak amplitudes and splittings. The ranges of solution for both

TABLE I

SOLUTION RANGES FOR THE POLARIZED EPR SPECTRUM OBSERVED WHEN X IS REDUCED PRIOR TO FLASHING

Model	$g_{P\text{-}700^+}$	$g_{A_1^-}$	J (G)
$A_1^- = [\text{Chl } a]_2^-$	2.0026	2.0031 ± 0.0002	1–3
$A_1^- = [\text{Chl } a]^-$	2.0026	2.0035 ± 0.0002	>1

dimer and monomer anion models are given in Table I.

The idea that the spectrum of Fig. 7 arises from a convolution of polarized P-700$^+$ and A_1^- spectra was tested by generating the polarized A_1^- spectrum and adding it to the calculated polarized P-700$^+$ spectra of Fig. 9. The spectrum of polarized A_1^- is generated in the same manner as that of P-700$^+$ except that the sum in Eqn. 9 is over the hyperfine states of A_1^- and the sign of $\bar{\rho}_i$ is opposite to that used in the P-700$^+$ case. In both cases ($A_1^- = [\text{Chl } a]_2^-$ and $A_1^- = \text{Chl } a^-$) unsatisfactory simulations of the experimental data were obtained. The problems with the simulations obtained under the assumption that both radicals are observed is that the splittings between the peaks are too large and that the asymmetry between the two negative lobes of the spectrum is diminished. The loss of asymmetry in the predicted spectra is probably a consequence of the fact that the sum of the overall polarization on both radicals must add up to zero. Therefore, we conclude that the spectrum of Fig. 7 is probably due to P-700$^+$ alone.

Two-site model

For experiments where X is not reduced prior to flashing, spin polarization can develop on P-700$^+$ due to spin-spin interactions between P-700$^+$ and A_1^- upon initial charge separation and between P-700$^+$ and X^- after electron transfer from A_1^- to X has occurred. Because we could not simulate the polarized spectrum of Fig. 2 with a one-site model and because we observed a significant dependence of the polarized signal on the orientation of broken chloroplasts, we conclude that a significant spin-spin interaction between P-700$^+$ and X^- does exist and that polarization on P-700$^+$ develops because of subsequent interactions with A_1^- and X^-. In this section a brief description of the two-site model for development of spin polarization in membrane-

bound systems following the proposals of Friesner et al. [9] will be given. Then the model will be applied to simulate the spectrum of Fig. 2.

For this model one follows the same procedure for calculating the polarization on the donor radical that we used in the one-site case. However, now we are interested in the polarization after the second radical pair has existed for some time, τ_2. A more general expression for $\rho(t)$ must be utilized here because a significant amount of S-T_0 mixing occurs prior to the formation of the second radical pair. If we take $|\psi(0)\rangle = C_S(0)\ |S\rangle + C_T(0)\ |T_0\rangle$ and follow the above procedure, one finds that the polarization on the donor radical is given by

$$\begin{aligned}\rho_{D^+}(t) = {} & [C_T(0)\, C_S^*(0) + C_T^*(0)\, C_S(0)] \\ & \{\cos^2\omega t + [(H_{AD}^2 - J^2)/\omega^2]\sin^2\omega t\} \\ & + (iJ/\omega)[C_T(0)\, C_S^*(0) - C_T^*(0)\, C_S(0)]\sin(2\omega t) \\ & + 2(JH_{AD}/\omega^2)\sin^2\omega t[|C_S(0)|^2 - |C_T(0)|^2] \end{aligned} \quad (12)$$

For the one-site model we took $C_S(0) = 1$, $C_T(0) = 0$ and obtained Eqn. 7. In the two-site case C_S and C_T in Eqn. 12 are the coefficients of $|S\rangle$ and $|T_0\rangle$ at the beginning of the time interval of constant J_2 ($t = t_1$). These coefficients may be obtained by suitable rearrangement of Eqn. 6 and inserted into Eqn. 12 to obtain

$$\begin{aligned}\rho_{D^+}(t_1, t_2) = {} & (2H_1J_1/\omega_1^2)\sin^2\omega_1 t_1 \\ & \cdot [1 - (2J_2^2/\omega_2^2)\sin^2\omega_2 t_2] \\ & + (J_2H_1/\omega_1\omega_2)\sin(2\omega_1 t_1)\sin(2\omega_2 t_2) \\ & + (2H_2J_2/\omega_2^2)\sin^2\omega_2 t_2 \\ & \cdot [1 - (2H_1^2/\omega_1^2)\sin^2\omega_1 t_1] \end{aligned} \quad (13)$$

Averaging over the lifetimes of the two radical pairs, t_1 and t_2, one obtains:

$$\begin{aligned}\rho_{D^+}(\tau_1, \tau_2) = {} & [4H_1J_1\tau_1^2/(1 + 4\omega_1^2\tau_1^2)] \\ & \cdot [1 - 4J_2^2\tau_2^2/(1 + 4\omega_2^2\tau_2^2)] \\ & + [4J_2H_1\tau_1\tau_2/(1 + 4\omega_1^2\tau_1^2)] \cdot [1/(1 + 4\omega_2^2\tau_2^2)] \\ & + [4H_2J_2\tau_2^2/(1 + 4\omega_2^2\tau_2^2)] \\ & \cdot [1 \quad 4H_1^2\tau_1^2/(1 + 4\omega_1^2\tau_1^2)] \end{aligned} \quad (14)$$

where J_1 and J_2 are the values of the exchange integral for radical pair 1 and 2, H_1 and H_2 the off-diagonal elements H_{AD} in each case, $\omega_1 = (H_1^2 + J_1^2)^{1/2}$, $\omega_1 = (H_2^2 + J_2^2)^{1/2}$, and τ_1 and τ_2 the lifetimes of each radical pair.

The orientation dependence of the polarization arises from the g-tensor anisotropy of X^- and enters into Eqn. 14 through the term H_2. Friesner et al. [9] developed an approximate expression for H_2 in this case. For hyperfine line i of P-700$^+$ it is given by:

$$\begin{aligned} H_2^i(\theta, \phi) = {} & \tfrac{1}{2}\beta|H|[g^{(P\text{-}700^+)} - (g_x^{(X^-)}\sin^2\theta\cos^2\phi \\ & + g_y^{(X^-)}\sin^2\theta\sin^2\phi \\ & + g_z^{(X^-)}\cos^2\theta)] + \tfrac{1}{2}A_i^{(P\text{-}700^+)}m_{iz} \end{aligned} \quad (15)$$

where $|H|$ is the magnitude of the applied magnetic field, and θ and ϕ the spherical polar angles that define the direction of H_0 in the principal axes system of the X^- g tensor. The polarization of hyperfine line i on the donor species is an ensemble average over all possible orientations of the reaction center with respect to H_0. For a randomly oriented sample this average is given by

$$\bar{\rho}_i = (2/\pi)\int_0^{\pi/2}\int_0^{\pi/2}\rho_i(\theta, \phi)\sin\theta\, d\theta\, d\phi \quad (16)$$

where $\bar{\rho}_i(\theta,\phi)$ is generated by using Eqns. 15 and 10 in Eqn. 14 and averaging over the hyperfine states of A_1^- as before. For magnetically aligned samples, $\sin\theta$ in the integrand of Eqn. 16 is replaced by a distribution function, $P(\theta,\phi)$ which describes the probability that the radicals possess a given orientation (θ,ϕ) relative to H_0. The EPR spectrum of polarized P-700$^+$ is then calculated using Eqn. 9 as in the one-site case.

Characterization and application of the two-site model

Attempts at simulating the spectrum of Fig. 2 using the two-site model were made for two specific cases. In the first case A_1 was assumed to be a Chl *a* monomer and g values and hyperfine coupling con-

stants which gave good solutions for the case where X was reduced prior to flashing (one-site case) were used in the simulations. In the second case A_1 was taken to be a Chl *a* dimer and *g* values and hyperfine coupling constants were chosen in the same manner as for the monomer. In both cases a *g* value of 2.0026 was used for *P*-700$^+$ and *g* values of 1.78, 1.88 and 2.08 [11] were used for X^-. The hyperfine coupling constants for *P*-700$^+$ were taken from the literature as they were in the previous case [24]. Values of J_1, the exchange coupling constant for the *P*-700$^+A_1^-$ radical pair, were taken from the ranges of solution determined for the experiments where X was reduced prior to flashing (Table I). The parameters which are not fixed from the above calculations are the lifetimes of the radical pairs, τ_1 and τ_2, and the exchange coupling constant between *P*-700$^+$ and X^-, J_2. τ_2 was found to have little effect on the simulations, since it is always much greater than τ_1 when charge transfer beyond X is blocked (the lifetime of X^- under our experimental conditions has been reported to be 100 ms [20]). In contrast, we found that the predicted lineshape was very sensitive to the values of τ_1 and J_2. This is what one might expect, because these parameters (τ_1 and J_2) control the relative amounts of *P*-700$^+A_1^-$ and *P*-700$^+X^-$ character that contribute to the predicted polarization pattern.

The effects of varying τ_1 on the predicted polarized *P*-700$^+$ spectrum are shown in Fig. 11. For small values of τ_1 (Fig. 11a), a completely emissive signal primarily due to interactions between *P*-700$^+$ and X^- is predicted. For long τ_1 values (Fig. 11c), a polarization pattern similar to that obtained in experiments where charge transfer to X was blocked is predicted. When τ_1 is between these two extremes (Fig. 11b), a mixture of these two patterns, similar to that obtained in our experiments, is obtained. We also noted that, if J_2 is of the same order of magnitude as J_1, the contribution from interactions between *P*-700$^+$ and X^- dominates the predicted spin polarization on *P*-700$^+$.

The best simulations of the spectrum of Fig. 2 (randomly oriented chloroplasts, X not reduced) assuming A_1 to be either a Chl *a* dimer or monomer are shown in Fig. 12. We found that the predicted relative peak amplitudes and splittings are in better agreement with the data if A_1 is taken to be a Chl *a* dimer species. Fig. 12 shows that for the case where

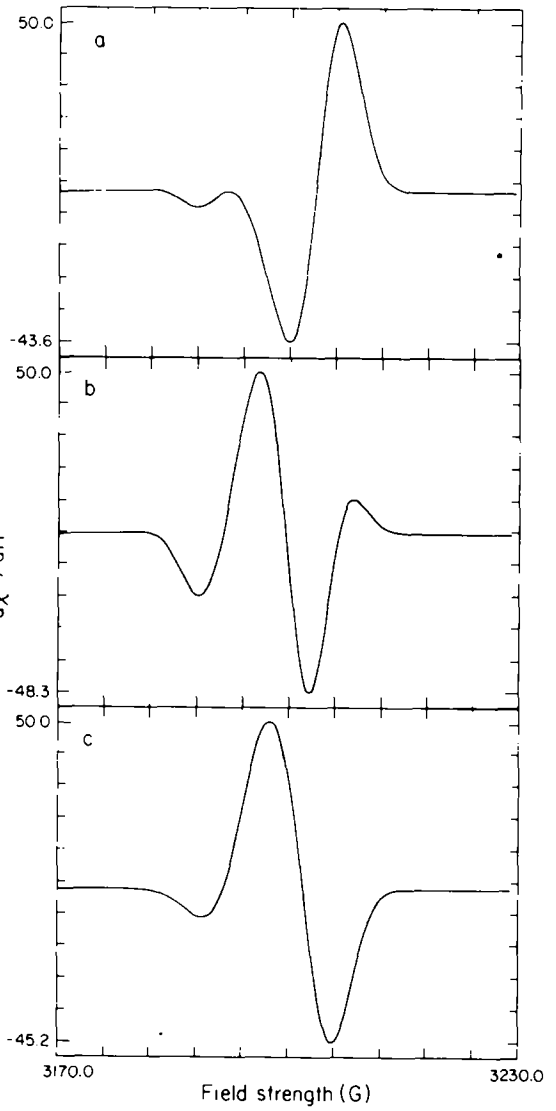

Fig. 11. Computer simulations of the spin polarized *P*-700$^+$ lineshape using a two-site model, for different values of τ_1. A_1 was taken to be a Chl *a* dimer species in this calculation. The *g* values and hyperfine coupling constants of *P*-700$^+$ are as in Fig. 10 and the *g* value and hyperfine coupling constants on A_1^- are as for Fig. 10b. The g values used for the X^- species are: g_x 1.78, g_y 1.88; g_z 2.08. The other parameters which are constant for the three simulations are J_1 = 2.0 G, J_2 = 0.03 G and τ_2 = 0.1 s. For a, τ_1 = 10 ps; for b, τ_1 = 800 ps; and for c, τ_1 = 10 ns.

A_1 is assumed to be a Chl *a* monomer neither the relative peak amplitudes nor the splittings between the peaks are predicted satisfactorily. We did find,

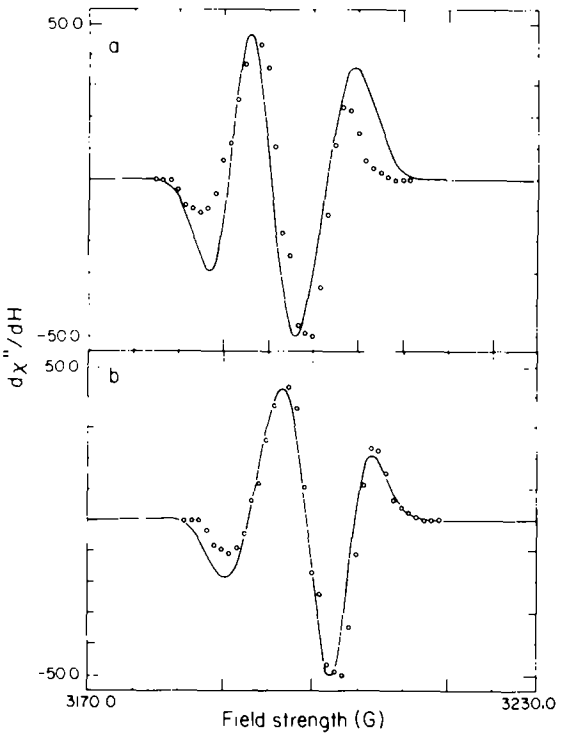

Fig. 12. A comparison of calculated and experimental EPR spectra for the data of Fig. 2 assuming A_1^- is a Chl *a* monomer (a) or a Chl *a* dimer species (b). The *g* values and hyperfine coupling constants used for *P*-700$^+$ are as for Fig. 10, and the *g* values used for the X species are as for Fig. 11. In a, A_1^- is taken to be a Chl *a* monomer species; its *g* value and hyperfine coupling constants are as for Fig. 10a. Other parameter values for a are $J_1 = 2.0$ G, $J_2 = 0.20$ G, $\tau_1 = 800$ ps and $\tau_2 = 0.1$ s. In b, A_1^- is taken to be a Chl *a* dimer species and the *g* value and hyperfine parameters are as in Fig. 10b. Other parameter values for b are $J_1 = 2.0$ G, $J_2 = 0.035$ G, $\tau_1 = 800$ ps and $\tau_2 = 0.1$ s. In a, the experimental points were shifted downfield 2 G to correlate with the predicted lineshape.

however, that the relative peak amplitudes in the monomer case can be simulated reasonably well if the hyperfine coupling constants on *P*-700$^+$ are narrowed by about 15%, but that the peak-to-peak splittings are still incorrect. For both sets of simulations we found that lineshapes similar to those of Fig. 2 can be obtained for $\tau_1 = 500-1100$ ps and $J_2 = 0.01-0.25$ G only if the ranges of the other parameters (*g* values, hyperfine coupling constants, J_1) used in the simulation are those needed to simulate the data obtained when X was reduced prior to flashing (one-site case). Also, for low values of τ_1 (500 ps) small values for J_2 are required (0.01–0.05 G) while for longer τ_1 values (1.0 ns), J_2 must be set at about 0.20 G. Similar results were obtained when slightly different *g* values for X^- [15,17] were utilized in these calculations.

As stated above, we also found that the spin polarized signal obtained when X was not reduced prior to flashing was orientation dependent (Fig. 9). Upon examination of Fig. 9, one finds that this orientation dependence has the largest effect on the two 'lobes' of the spectrum at high field. The simulations of Fig. 11 show that this part of the spectrum is the one most influenced by the interactions between *P*-700$^+$ and X^-. We are currently studying this orientation effect in greater detail and computer simulations of these data will appear later.

Dynamics of the transient signals

An interesting feature of the transient EPR signals of Figs. 1 and 6 is the fact that the relaxation is dependent on redox potential. Upon prior reduction of X the half-life of the observed decay decreases by an order of magnitude. This is what one might expect to observe from a radical in close proximity to a fast-relaxing paramagnetic species (e.g., X^-), or if the dynamics reflect the back reaction of the radical pair.

The decay of electron spin polarization when monitored by continuous wave EPR techniques is a convolution of three processes [8,25]. The dominant process at high microwave powers can be stimulated emission or absorption of microwave radiation [25]. The other processes are spin lattice relaxation and chemical decay of the radical pair. Thus, the observed decay rate is a convolution of rates of differing magnitude. The relative contributions of these processes can be sorted out as described by Atkins et al. [8], by studying the microwave power dependence of the decay dynamics. In the absence of chemical relaxation and distortions due to magnetic field modulation [26], the transient solutions to the Bloch equations predict a simple exponential decay with decay constant given by:

$$k_{\text{eff}} = 1/T_{\text{eff}} = 1/T_1 + (\gamma H_1)^2 T_2'(1 + \delta\omega^2 T_2^2) \qquad (17)$$

where T_1 and T_2 are the spin-lattice and spin-spin relaxation times, γ the gyromagnetic ratio, H_1 the

magnitude of the microwave field and $\delta\omega$ the frequency offset from resonance. The assumptions made in the derivation of Eqn. 17 are $T_1 >> T_2$ and $\delta\omega \neq 0$. Eqn. 17 predicts that a plot of the observed decay constant vs. microwave power (which is proportional to H_1^2) will yield a straight line. Extrapolation to zero power will give a value for T_1. The linearity of a plot of the effective decay constant at low microwave power provides evidence for the validity of the assumption that chemical decay is not important.

The spin polarized signals from spinach chloroplasts with only Fd_B and Fd_A reduced (Fig. 1) are slow enough at low temperature so that they can be time resolved with our instrument. The power dependence of the effective rate of this decay is shown in Fig. 5. It is nearly linear, apparently because the chemical decay rate is significantly slower than the spin relaxation rate in this case [20]. Extrapolation to zero power gives a T_1 of 60 μs.

Preliminary studies on the slower kinetic component (Fig. 4) arising in spinach chloroplasts prepared in this same redox state show a nonlinear dependence on microwave power, suggesting that chemical decay is contributing at longer times. Future studies will focus on extracting the relative contributions of each of the dynamical processes from the effective decays of the spin-polarized transients as a function of redox potential, temperature and microwave power.

Conclusions

In this work we examined the effect of a pulse of light in developing spin polarization on $P\text{-}700^+$ from spinach chloroplasts and PS I particles poised in two different redox states. In the first state, chloroplasts were treated so that the species X was reduced, thus blocking electron transfer from A_1 to X. In this case the polarized lineshape of $P\text{-}700^+$ was of a mixed emission-enhanced absorptive type (Fig. 7). Using the radical pair theory of CIDEP adapted by Friesner et al. [9] for membrane-bound systems, we obtained computer simulations of these data (Fig. 10) for cases where A_1 was assumed to be a Chl *a* monomer or where A_1 was taken to be a Chl *a* dimer species. Both models fit the data within experimental error. An important feature of the simulations of Fig. 10 is that the center of the spectrum for the monomer case is shifted about 2 G downfield relative to that of the dimer case. Because our experimental uncertainty in *g* values is ±0.001, the experimental points in Fig. 10a were moved in the monomer case to correlate better with the simulation.

Chloroplasts poised in a redox state where X is not reduced prior to flashing give rise to the spectrum of Fig. 2. We attempted to simulate this signal with a two-site model [9] assuming A_1 to be either a monomer or a dimer of Chl *a* (Fig. 12). The monomer model is unsatisfactory in this case because the polarization due to $P\text{-}700^+A_1^-$, when convoluted with that arising from $P\text{-}700^+X^-$, gives a lineshape distorted from that obtained experimentally. The primary reason for the distortion in the monomer case, but not the dimer case, is the 2 G shift to lower field strength mentioned above. Therefore, our data suggest that A_1 is a Chl *a* dimer species rather than a monomer.

Our proposal that A_1 is a Chl *a* dimer species is in disagreement with recent reports in the literature [14, 18,19,23]. In these reports, the authors observed a light-induced, reversible EPR signal in the *g* 2.00 region from several types of PS I preparation which were either poised at low redox potentials or treated with detergents to remove X and the iron-sulfur proteins. Consequently, these authors conclude that the light-induced steady-state EPR signal is due to reduced A_1. Because this signal is broad (linewidth approx. 14 G), they conclude that A_1 is a Chl *a* monomer species or a pheophytin *a* monomer [19]. However, no quantitive EPR work was done to determine the stoichiometry between the species giving rise to the broad signal and the PS I reaction center. Also, no studies on the effects of the amplitude of the broad signal on the primary photochemistry were done.

Recent work by McLean and Sauer [27] shows that for spinach chloroplasts and PS I reaction centers prepared with Triton X-100, there is no dependence of the yield of the radical pair polarized triplet [22] (formed from the back reaction between $P\text{-}700^+$ and A_1^-) on the amplitude of the broad *g* 2.00 signal discussed above. These authors also examined PS I reaction centers which lacked X and iron-sulfur centers A and B. For these samples they found that as the amplitude of the broad *g* 2.00 signal was increased, by longer illumination periods prior to freezing, the amplitude of the radical pair polarized triplet signals decreased in agreement with

previous reports [28]. We conclude that much of the EPR signal observed in this region is due to the photodegradation of light harvesting or antenna chlorophyll and that the portion due to A_1^- is masked.

Acknowledgements

The authors wish to acknowledge many helpful discussions with M.P. Klein, R. Friesner, and M.B. McLean. This work was supported by the Director, Office of Energy Research, Office of Basic Energy Sciences, Division of Biological Energy Conversion and Conservation of the U.S. Department of Energy under Contract No. W-7405-ENG-48, a grant from the National Science Foundation (PCM79-11251) and an N.I.H. National Research Service Award to H.A.F.

References

1 Blankenship, R., McGuire, A. and Sauer, K. (1975) Proc. Natl. Acad. Sci. U.S.A. 72, 4943–4947
2 Dismukes, G.C., McGuire, A., Blankenship, R. and Sauer, K. (1978) Biophys. J. 21, 239–256
3 McIntosh, A.R., Manikowski, H., Wong, S.K., Taylor, C.P.S. and Bolten, J.R. (1979) Biochem. Biophys. Res. Commun. 87, 605–612
4 McIntosh, A.R., Manikowski, H. and Bolton, J.R. (1979) J. Phys. Chem. 83, 3309–3313
5 McIntosh, A.R. and Bolton, J.R. (1976) Nature 263, 443–445
6 Thurnauer, M.C., Bowman, M.K. and Norris, J.R. (1979) FEBS Lett. 100, 309–312
7 Hoff, A.J., Gast, P. and Romijn, J.C. (1977) FEBS Lett. 73, 185–190
8 Atkins, P.W., McLauchlan, K.A. and Percival, P.W. (1973) Mol. Phys. 25, 281–296
9 Friesner, R., Dismukes, G.C. and Sauer, K. (1979) Biophys. J. 25, 277–294
10 Sauer, K., Mathis, P., Acker, S. and Van Best, J.A. (1978) Biochim. Biophys. Acta 503, 120–134
11 Evans, M.C.W., Sihra, C.K. and Cammack, R. (1976) Biochem. J. 158, 71–77
12 Ke, B. (1973) Biochim. Biophys. Acta 301, 1–33
13 Malkin, R. and Bearden, A.J. (1971) Proc. Natl. Acad. Sci. U.S.A. 63, 16–19
14 Heathcote, P., Timofeev, K.N., Evans, M.C.W. (1979) FEB Lett. 101, 105–109
15 McIntosh, A.R. and Bolton, J.R. (1976) Biochim. Biophys. Acta 430, 555–559
16 Hiyama, T., Tsujimoto, H.Y. and Arnon, D.I. (1979) FEBS Lett. 98, 381–385
17 Dismukes, G.C. and Sauer, K. (1979) Biochim. Biophys. Acta 504, 431–445
18 Heathcote, P. and Evans, M.C.W. (1980) FEBS Lett. 111, 381–385
19 Baltimore, B. and Malkin, R. (1980) Photochem. Photobiol. 31, 485–490
20 Shuvalov, V.A., Dolan, E. and Ke, B. (1979) Proc. Natl. Acad. Sci. U.S.A. 76, 770–773
21 Adrian, F. (1971) J. Chem. Phys. 54, 3918–3923
22 Frank, H.A., McLean, M.B. and Sauer, K. (1979) Proc. Natl. Acad. Sci. U.S.A. 76, 5124–5128
23 Fujita, I., Davis, M.S. and Fajer, J. (1978) J. Am. Chem. Soc. 100, 6280–6282
24 Sheer, H., Katz, J.J. and Norris, J.R. (1977) J. Am. Chem. Soc. 99, 1372–1381
25 Gast, P. and Hoff, A.J. (1978) FEBS Lett. 85, 183–188
26 Friesner, R., McCracken, J.L. and Sauer, K. (1981) J. Magn. Resonance 43, 343–356
27 McLean, M.B. and Sauer, K. (1982) Biochim. Biophys. Acta 679, in the press
28 Rutherford, A.W. and Mullet, J.E. (1981) Biochim. Biophys. Acta 635, 225–235